ORIGINAL RESEARCH

Novel Self-assembly Pd(II)-Schiff Base Complex Modified Glassy Carbon Electrode for Electrochemical Detection of Paracetamol

Mahmoud A. Hefnawy[1] · Shymaa S. Medany[1] · Sahar A. Fadlallah[1] · Rabab M. El-Sherif[1] · Safaa S. Hassan[1]

Abstract

A self-assembly Pd-Schiff base complex was synthesized and used as an electrochemical sensor in phosphate buffer solution, where it enhanced the electrocatalytic activity toward the paracetamol detection. The Schiff base {(HL) = (4-(((Z)-3-(hydroxyimino) butan-2-ylidene) amino)-1,5-dimethyl-2-phenyl-1,2-dihydro-3H-pyrazol-3-one)} was selected to prepare Pd-based complexes due to its high antimicrobial activity. A linear calibration curve was constructed using GC/Pd-SB in paracetamol concentration range of 1–50 μM and its detection limit was calculated as 0.067 μM. The modified electrode, GC/Pd-SB, could successfully determine the paracetamol concentration in human blood serum and commercial drug tablets with high sensitivity. The prepared metal complex was characterized using techniques, namely, X-ray diffraction (XRD) and scanning electron microscope (SEM). In addition, electrochemical studies were performed using different electrochemical techniques like cyclic voltammetry (CV), linear sweep voltammetry (LSV), chronoamperometry (CA), and electrochemical impedance spectroscopy (EIS). DFT calculations were used to estimate the equilibrium geometry, molecular orbital, ground-state properties, and interaction energy between paracetamol and palladium.

Keywords Self-assembly Pd (II) complexes · Schiff base · Paracetamol detection · Electrochemical sensor · Drug sensor

Introduction

Paracetamol (N-acetyl-P-aminophenol, PS) is an analgesic and antipyretic drug frequently used for pain removal, including migraine headaches, muscular aches, and chronic pain [1–3]. The excess dose of PS leads to toxic metabolite accumulation, thereby damaging the kidneys and liver [1, 4].

Several methods were employed for sensing paracetamol in biological systems, such as liquid chromatography-mass spectrometry (LC–MS) [5–7], chemiluminescence [8–10], high-performance liquid chromatography (HPLC) [11–14], spectrofluorimetry [15–17], and electrochemical techniques [18–21].

Electrochemical detection, one of the vital techniques, is widely used to detect drugs, neurotransmitters, and metal ions due to relatively faster, cheaper, higher sensitivity, and selectivity than other detection techniques [22, 23].

Voltammetry is considered a highly sensitive electrochemical technique for detecting the trace amounts of pharmaceutical compounds. The pharmaceutical compounds are biological molecules with chemically active functional groups that can undergo redox processes, and their redox activity can be estimated by several voltammetry techniques like cyclic voltammetry, linear sweep voltammetry, and differential pulse voltammetry.

Schiff bases are organic compounds synthesized by condensing ketones and/or aldehyde with primary amines to give an imine group. The electronic properties of the Schiff base can be tuned by changing the amine and substituted carbonyl compound [24, 25]. The Schiff base metal complexes were found to be applicable in different research fields like their reversibility with oxygen binding [26, 27], efficient hydrogenation of olefins [28, 29], high ability to form a complex with some toxic metals [30, 31], and the high ability to detect prohibited drugs and explosive [32–37].

4-Aminoantipyrine-based heterocyclic, a derivative of antipyrine, has been used for various medical applications such as protection against oxidative stress and prophylactic of some diseases, including cancer [38]. Otherwise, the oxime-derived compounds and their metal complexes have

✉ Shymaa S. Medany
   shymaasamir80@cu.edu.eg; shymaasamir80@yahoo.com;
   shymaa@sci.cu.edu.eg

1   Chemistry Department, Faculty of Science, Cairo University,
    12613, Giza, Egypt

Scheme 1 Schematic diagram of Pd-Schiff base preparation steps
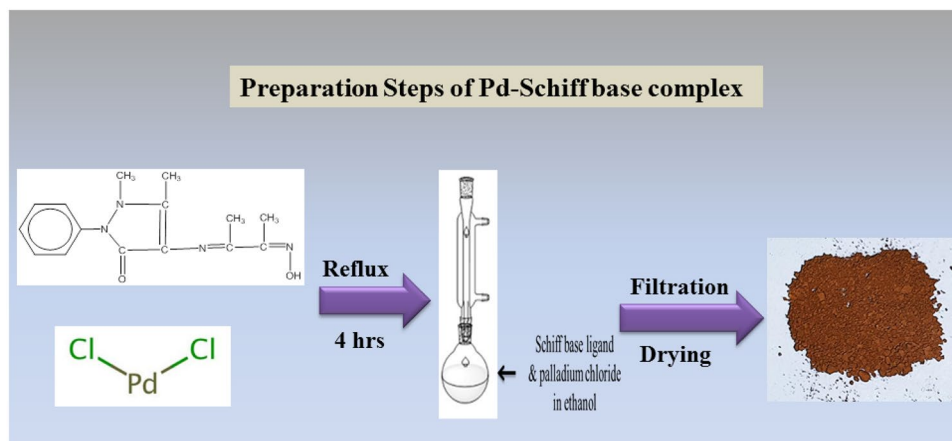
been reported as important constituents in many biological and medical applications like electrochemical sensors [39, 40].

The noble metal-based catalysts have gained significant research interest, whereas the high catalytic selectivity was achieved by tuning the use of the noble metals in many sensing applications [41, 42]. Therefore, complexes based on palladium metal are reported as catalysts for electrochemical sensors. Polybithiophene-palladium and EDOT-substituted bis(2-pyridylimino)isoindolato-palladium complexes were used as a glucose sensor [43, 44], and pyridine-2,6-dicarboxamide-palladium was used for the detection of an anticoagulant drug [45].

In the present work, a palladium-Schiff base complex prepared previously [46] was used in electrochemical sensor applications. The modified electrode was investigated for electrochemical detection of paracetamol in a phosphate buffer solution. The electrochemical activity of the electrode was studied in different ranges of pH. The kinetic parameters like the diffusion coefficient of paracetamol were calculated. Also, the sensor anti-interference ability and longtime stability for paracetamol determination are performed. The equilibrium structure and some of the ground-state properties were established using DFT calculations. The adsorption of the paracetamol molecule was studied over different facets of Pd surfaces.

Experimental

Materials

All chemicals are analytical grades and were used as received without further purification. Potassium phosphate (mono, di-basic salts), potassium hydroxide (KOH), ethanol, palladium chloride ($PdCl_2$), diethyl ether, 4-aminoantipyrine, 2,3-butanedione monoxime, dimethylformamide (DMF), and paracetamol were purchased from Sigma-Aldrich.

Phosphate buffer solution, PBS (1.0 M K_2HPO_4 and 1.0 M KH_2PO_4) of pH 4–9, was used as a supporting electrolyte. The pH was adjusted using suitable amounts of 0.1 M H_3PO_4 and 0.1 M KOH. All solutions were prepared using double-distilled water, and dilutions were prepared from stock solutions.

Preparation of Palladium Complex

Preparation of Schiff Base (SB)

The Schiff base was prepared as follows: firstly, in the flask (A) solution, 4-aminoantipyrine was prepared by dissolving 10 mmol of 4-aminoantipyrine in 25 mL of ethanol. In flask (B), 10 mmol of 2,3-butanedione monoxime was dissolved in ethanol. Both solutions were then stirred, and the temperature was increased gently. After this, the two solutions were mixed to obtain a new mixture by adding flask (A) solution dropwise to flask (B) solution. Afterward, the mixture was left under a flux condition system for 4 h. Finally, the yellow Schiff base product was filtered, washed, recrystallized, and dried.

Synthesis of Pd Complex (Pb-SB) and Self-assembly Metal Complex

As represented in Scheme 1, the metal complex of the Schiff base, HL, was prepared as follows: in the beginning, a hot solution of 1 mmol palladium chloride, dissolved in a water–ethanol mixture (1.25:1 mL), was added to 25 mL of a hot solution of a water–ethanol mixture containing 1 mmol of Schiff base (1 L:1 Pd). Then, the obtained mixture was stirred under reflux for 2 h. Once the palladium complex was precipitated, the obtained complex was collected by filtration and washing thoroughly with hot ethanol followed by diethyl ether until the color became colorless. After this, the obtained complex was kept in vacuum desiccators over anhydrous calcium chloride. Lastly, the self-assembly Pd-SB

was prepared using the evaporation method by dissolving 10 mg of the as-prepared complex in 1 mL of dimethylformamide, DMF, then the complex ink was cast on the electrode, and DMF was left to dry in the ambient air for 4 h.

Structure and Morphology Analysis

The Pd-Schiff base complex sample structures were characterized using X-ray diffraction (XRD) by Analytical X'Pert using Cu-Kα radiation ($\lambda = 1.5406$ Å). The microstructure of the samples was investigated using Quanta FEG 250 (USA) instrument and an EDAX Unit (energy-dispersive X-ray analyses) coupled to SEM with accelerating voltage 30 kV and magnification $14 \times$ up to $1{,}000{,}000 \times$ and resolution for Gun. This instrument was used to analyze the composition of the prepared samples. A GC was modified with a Pd-Schiff base before and after casting. The samples were coated with gold using EMITECH k550x sputter coater to enhance the samples' conductivity and resolution.

Electrode Fabrication and Electrochemical Measurements

The electrochemical measurement was investigated using a glassy carbon electrode (3 mm in diameter) as a working electrode. Ten milligrams of Pd complex was suspended in 1 mL DMF, and the solution was sonicated for 1 h to ensure the obtaining of complete homogenous catalyst ink. Then, 20 μL of catalyst ink was cast on a 0.3 mm (0.0707 cm^2) glassy carbon electrode, and the electrode was left to dry overnight. The electrochemical measurement was performed in the standard three-electrode system using Ag/AgCl/KCl (sat.) as the reference electrode and Pt wire as the auxiliary electrode. Phosphate buffer solution (PBS) was used as an electrolyte at different pH values. Linear sweep voltammetry (LSV), constant potential chronoamperometry (CA), and electrochemical impedance spectroscopy (EIS) were performed using Autolab potentiostat/galvanostat PGSTAT128N, while the fitted circuit was done using Nova (Version 2.1, Metrohm Autolab, Utrecht, Netherlands). A three-electrode cell was constructed with the prepared electrocatalysts, Ag/AgCl/KCl (sat.), Pt wire as working, reference, and auxiliary electrodes, respectively. All potential values in this work were referred to Ag/AgCl/KCl (sat.) reference electrode.

A constant AC voltage value was adjusted during the electrochemical impedance spectroscopy measurements by applying an AC voltage amplitude of 10 mV and a frequency range from 1×10^4 to 0.1 Hz. The obtained data were fitted to a chosen electric circuit model using a complex non-linear least squares (CNLS) circuit fitting software. All electrochemical studies were carried out at room temperature.

Computational Method

The geometry optimization for Schiff base ligand and metal complex was estimated using density functional theory (DFT). Thus, the calculations have been carried out to investigate the equilibrium geometry of Schiff base (free ligand) and Pd-SB (metal complex) using Gaussian 09 program [47] at the B3LYP/6-311G and B3LYP/LANL2DZ level of theory for Schiff base and Pd-SB respectively.

The interaction between paracetamol and palladium center has been implemented using the generalized gradient density approximation (GGA) in the revised Perdew-Burke-Ernzerhof parameterization, RPBE, modified by Hammer et al. [48]. Calculations were done using the Cambridge Serial Total Energy Package [49], CASTEP, and employed ultrasoft pseudo-potentials. The adsorption process is modeled on a 3-layer supercell slab, separated by the vacuum of 10-Å thicknesses. The algorism employed for atomic relaxation was Broyden–Fletcher–Goldfarb–Shanno (BFGS). The three-layer atoms were adjusted as the two bottom layer atoms were fixed and the other top one was relaxed. The cells with periodic boundary conditions were used to achieve all calculations. A 2×2 supercell was designed for DFT calculations. The maximum force of convergence measurement for the geometry optimizations was 0.05 eV/Å with energy 2.0×10^{-5} eV/atom. The energy cut-off has been fixed for all surfaces at 340 eV. Else, the Monkrokhst-Pack scheme was used for utilizing Brillion zone integrations [50]. The k-point sampling is varied while performing energy calculations for the isolated paracetamol molecule, clean surfaces, and paracetamol-substrate complexes at different facets. The converged k-point samplings used were $(2 \times 2 \times 1)$ and $(2 \times 2 \times 2)$ for the ((100), (110), and (111) surfaces) and (free paracetamol), respectively.

Results and Discussion

Surface, Structural, and Spectral Characterization

The structure of the Pd-SB was characterized using powder X-ray diffraction (XRD). As shown in Fig. 1, XRD chart of the as-prepared Pd-SB was found to have amorphous criteria. Consequently, the broad peak was observed at $2\Theta \sim 20$. Otherwise, the XRD spectrum was performed for the Pd-SB after casting the catalyst ink on the GC electrode. The characteristic peak for Pd was observed (Fig. 1) at $2\Theta = 39.6$, 45.6, and 66.4 for corresponding indices (111), (200), and (220), respectively, based on JCPDS file no. 87–0638. The other observed peaks at $2\Theta = 6.26$, 8.12, 11.4, 13.2, and 14.38 correspond to the Pd-Schiff base [46, 51].

The surface morphology of the as-prepared Pd complex was characterized using a scanning electron microscope (SEM), as illustrated in Fig. 2a. It is clear from SEM
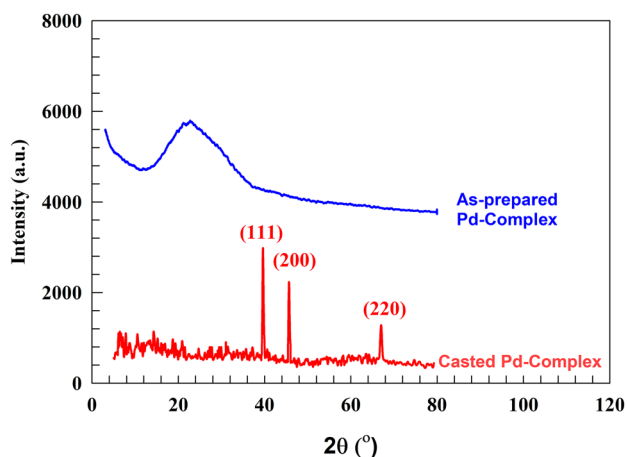
Fig. 1 XRD of the Pd-Schiff base complex as-prepared and after casting on GC electrode

image that the as-prepared Pd complex has a fused rod shape. Moreover, the crystal has a wide range of size distribution. Furthermore, the electrode surface was

studied after casting metal complex ink to prepare a self-assembled Pd-SB modified glassy carbon electrode. In Fig. 2b, c, the different magnifications of the Pd-Schiff base complex corresponding to polymerized metal complex layer on the surface of the electrode, a layer of metal complex was observed lake of crystallinity with tunnels across the surface. Figure 2d presents an image that illustrates tunnels through the surface. The elemental analysis was performed using SEM mapping, as given in Fig. S1, to represent the elemental distribution of Pb, N, C, O, Cl, and S. Thus, the percentage of each element corresponding to the EDAX analysis is listed in Table 1. Further characterization that proves the formation of metal complex was reported in previous work [46].

DFT Calculations

Density functional theory, DFT, is an essential tool used by researchers for enhancing work efficiency [52]. The theoretical models were employed for predicting geometry, electronic structure, and energy [53–55]. DFT also offers a
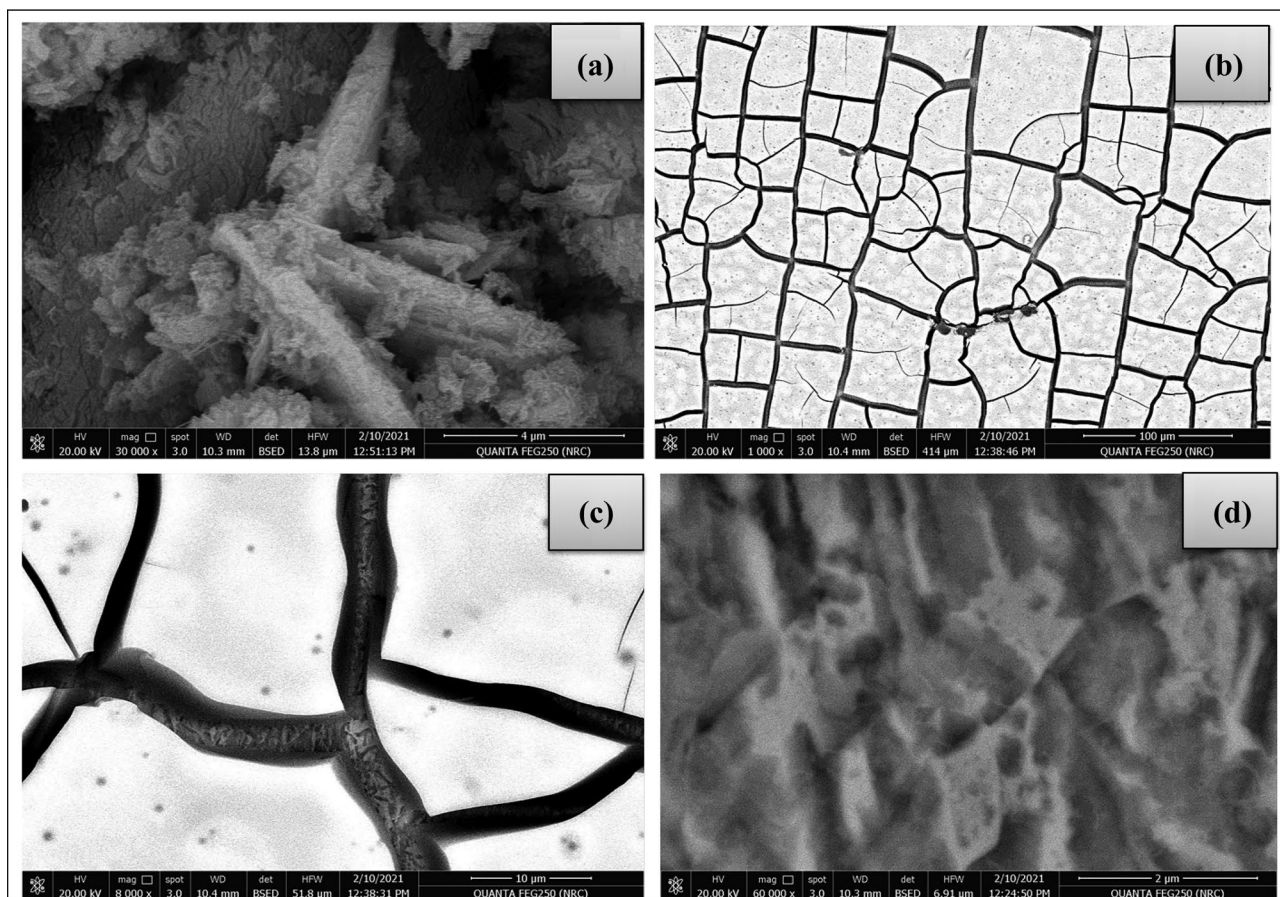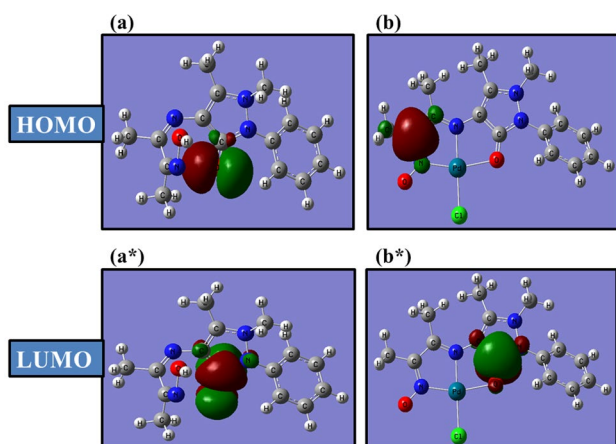

Fig. 2 SEM image of **a** as-prepared Pd-Schiff base, **b**, **c** different magnifications of self-assembly modified electrode GC/Pd (Schiff base), **d** high magnification of tunnel within the surface

Table 1 Elemental analysis based on mapping data

Element	Pd L	Cl K	O K	C K	N K	Pd L
Weight %	32.73	16.45	23.93	13.87	13.03	32.73

Fig. 3 The representation of highest occupied molecular orbitals (HOMO) and lowest unoccupied molecular orbitals (LUMO) molecular graphs of Schiff base ligand (**a**, **a***) and Pd-SB complex (**b**, **b***)

calculation method to study the interaction between the molecules and the surfaces [56–58]. Also, the adhesion phenomenon is an essential step for the electrochemical detection of drugs and was explained by various theories like mechanical interlocking theory, diffusion theory, electronic theory, and adsorption theory [59–62]. The adsorption theory describes the adhesion force acting between atoms in the interface region (the adsorbent and adsorbate) [62, 63].

The optimized structure of the Schiff base ligand and Pd-SB complex was estimated to calculate the ground-state properties, as given in Fig. S2. Figure 3 illustrates the corresponding energies of the highest occupied molecular orbital (HOMO) and lowest unoccupied molecular orbital (LUMO) for ligand (a, a*) and Pd complex (b, b*), respectively. Many ground-state parameters were studied, such as electron affinity, ionization potential, electronegativity, hardness, and dipole moment. The length of the Pd–O or Pd–N indicates that these bonds have a slightly ionic character where the bond criteria can be expressed by the bond length [64, 65].

Additionally, atomic charges, electron distribution of the frontier orbitals, and stabilizing electron transfers were

determined by Mulliken population analysis (MPA) and natural population analysis (NPA). The results for some selected atoms are pointed out in Table S1. For NPA results, the electron density of O13, N14, and N18 decreased in Pd-SB compared to Schiff base due to the transfer of charge from ligand to metal and the formation of a coordinate bond. Consequently, the value of charge upon complexation (−0.637), (−0.444), and (−0.159) was changed to (−0.635), (0.435), and (−0.010) for O13, N14, and N18, respectively. Table 2, reported the Ground-State properties of Schiff base (Free ligand), and Pd-Schiff base complex using B3LYP method.

The DFT calculation was used for studying the adsorption of paracetamol on palladium centers. For modeling and studying the adsorption energy, the electronic structure of paracetamol is first calculated as an isolated (free) molecule and then studied after adsorption within the palladium-paracetamol system. The adsorbate crystal was designed to study paracetamol adsorption on the Pd metal center. Then, the procedure is achieved for the (100), (110), and (111) surface facets. The interaction energy between paracetamol and Pd was calculated by subtracting the summation of the individual Pd, E_s, and paracetamol molecule energy, $E_{adsorbate}$, in a free state before adsorption from the total energy of the surface-adsorbate, $E_{(suf+adsorbate)}$, as represented in the following equation [66]:

$$E_{ads} = E_{(surf+adsorbate)} - E_s - E_{adsorbate} \tag{1}$$

Subsequently, more negative binding energy can represent a stronger interaction. Figure 4a–c represent the different facets of Pd crystals, namely (100), (110), and (111). The adsorption energy of paracetamol was calculated as (−0.802), (−0.473), and (−0.314) eV for $Pd_{(100)}$, $Pd_{(110)}$, and $Pd_{(111)}$ respectively. Therefore, the adsorption ability of paracetamol on the Pd center reflects the applicability of the Pd-based complex for the detection of paracetamol.

Moreover, the interaction between the analyte and the surface is an essential aspect of the electrochemical oxidation process. Therefore, the density of state was employed to understand the principle of adsorption of paracetamol (see

Table 2 Ground-state properties of Schiff base (free ligand), Pd-Schiff base complex using B3LYP/6-311G, and B3LYP/ LANL2D, respectively

Parameter	E_{Total} (Hartree)	Electron affinity[*] (eV)	Ionization potential[**] (eV)	Electronegativity[***] (eV)	Hardness[****] (eV)	Dipole moment (debye)
Schiff base	−951.75	0.012	0.242	0.127	0.115	4.0571
Pd-SB	−1092.81	0.080	1.860	0.970	0.890	17.3512

[*]Electron affinity=-LUMO; [**]ionization potential=-HOMO; [***]electronegativity (χ)=(HOMO+LUMO)/2; [****]hardness (η)=(LUMO−HOMO)/2
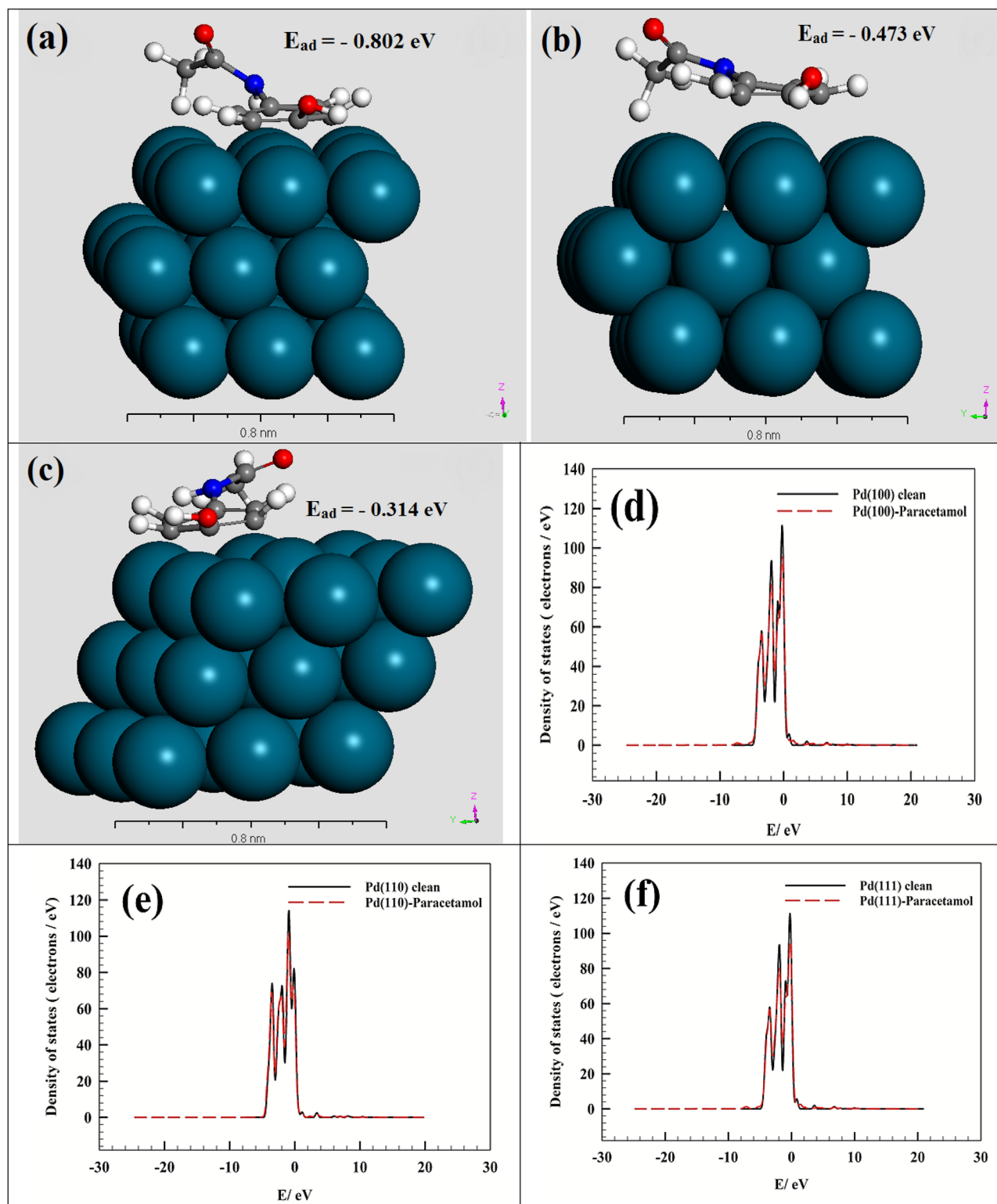
Fig. 4 **a** Paracetamol adsorbed on Pd(100), **b** paracetamol adsorbed on Pd(110), **c** paracetamol adsorbed on Pd(111). The partial density of state for d-orbitals of **d** Pd(100), **e** Pd(110), and **f** Pd(111)
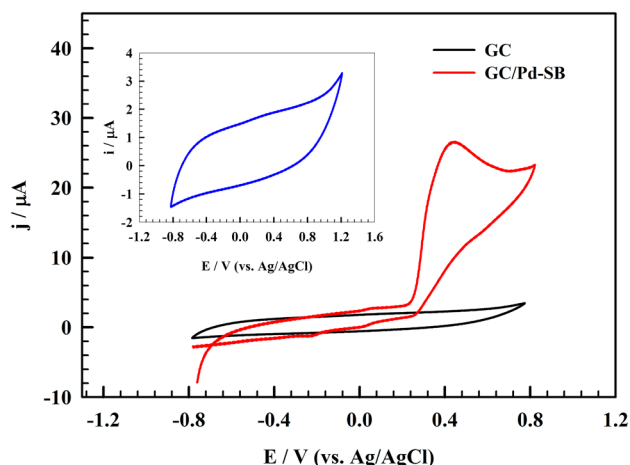
Fig. 5 CVs of GC/Pd-Schiff base for determination of 50 μM paracetamol at 0.1 M PBS (pH = 7.4) at scan rate 20 mV.s^{-1}

Fig. 4d–f). The chart shows the presentation of d-orbital for clean surface and paracetamol-Pd complex that the binding energy is decreased due to charge transfer from paracetamol molecule to the palladium surface. The density of states confirms the role of d-orbitals in the adsorption process.

Electrochemical Detection of Paracetamol

The electrochemical activity of GC/Pd-SB toward paracetamol was studied using the cyclic voltammetry technique.

Figure 5 shows the cyclic voltammograms of bare GC and the modified electrode, GC/Pd-SB, in 0.1 M PBS (pH = 7.4) containing 50 μM of paracetamol at 20 mV s^{-1} scan rate. The inset Fig. 5 represents the CV of the modified GC/Pd-SB in PBS in the absence of the paracetamol. Paracetamol voltammogram shows a prominent oxidation peak with a slightly small reduction peak at potentials of 500 and −100 mV, respectively. The bare GC voltammogram shows no significant peaks for paracetamol in the studied potential range, reflecting the ability of the self-assembly Pb-SB electrode to detect the paracetamol molecules. Paracetamol electrochemical oxidation was estimated as a two-electron and two-proton process, as shown in Scheme 2 [67].

The electrochemical impedance (EIS) was performed for the modified GC/Pd-SB electrode to study the charge transfer and solution resistance. Figure 6 shows the Nyquist plot of modified GC/Pd-SB in 0.1 M PBS (pH = 7.4) solution containing 50 μM paracetamol at the oxidation AC potential of 500 mV based on the maximum peak potential in the CV. The inset Fig. 6 represents the Nyquist plot of the modified electrode in PBS without the paracetamol. The EIS data were fitted to the equivalent circuit, inset Fig. 6, where Rs corresponds to the solution resistance, R_1 is the outer layer resistance, R_2 is the resistance of the inner layer of the electrode, C_1 is the capacitance of the outer layer, and C_2 is the capacitance element of the inner layer of electrode. W is a Warburg impedance parameter that represents the diffusion of the analyte. The parameters of fitted data are listed in Table 3. In the presence of paracetamol, the semicircle became more likely to describe the charge
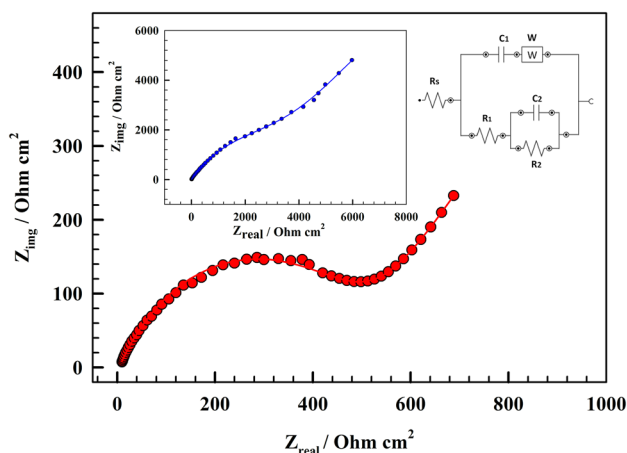
Scheme 2 **a** Representation of paracetamol oxidation, **b** Pd(II)-Schiff base complex

Fig. 6 EIS of the GC/Pd-SB electrode in the presence of 50 μM of paracetamol and 0.1 M PBS (pH = 7.4) at constant potential of + 500 mV (vs. Ag/AgCl). The inset figures: the Nyquist plot in the absence of the paracetamol and fitting circuit

transfer process than the inset Nyquist in PBS, which describes a diffusion process. Moreover, the charge transfer resistance of the electrode decreases due to the faradic process of paracetamol electrooxidation.

Effect of Paracetamol Concentration

Paracetamol is considered the most common, used, and important antipyretic drug. The permissible dose of paracetamol in serum should be below 30 mg/L (~ 200 μmol/L) to avoid paracetamol poisoning [68]. Therefore, the calibration curve of paracetamol detection and sensitivity was studied in the range of concentration suitable to the actual paracetamol concentration range. Accordingly, the effect of changing the paracetamol concentration was studied using the cyclic voltammetry (CV) technique (Fig. 7a). The calibration curve and sensitivity of the electrode were performed within the concentration range (1×10^{-6} up to 50×10^{-6} M) in a solution of 0.1 M PBS (pH = 7.4) at a scan rate of 20 mV s^{-1}.

As shown in Fig. 7b, the sensor was found to have a linear response as the following equations:

$$I_p \, (\mu A) = 0.372 C_{Paracetamol} \, (\mu M) + 5.68$$

Otherwise, the limit of detection and the limit of quantization were estimated using the calibration curve slope. The limit of detection is an analytical procedure that can estimate the minimum amount of analyte in a sample that can be detected [69]. On the other hand, the limit of quantization reflects the lowest drug concentration that can be detected quantitatively using a stated accuracy and precision [70].

The limits of detection (LOD) and limits of quantization (LOQ) were calculated for paracetamol according to the following equations:

$$LOD = 3 \, s/m, \text{ and } LOQ = 10 \, s/m$$

where s is the standard deviation and m is the slope of the calibration curves.

For GC/Pd-SB modified electrode, LOD and LOQ were found to be 0.067 and 0.223 μM, respectively.

Our work for paracetamol determination was compared with other electrodes found in the literature and mentioned in Table 4.

Diffusion and Scan Rate Effect and Kinetic Studies

The effect of the diffusion of paracetamol toward the electrode was measured as a function of different scan rates using the Randles–Sevcik equation as follows:

$$i_p = 2.69 \times 10^5 n^{3/2} A \, D^{1/2} C \, v^{1/2}$$

where i_p is the oxidation current (mA), n is the number of the electron ($n = 2$), A is the electrode surface area ($A = 0.0707$ cm^2), D is the diffusion coefficient, C is the bulk concentration (50×10^{-9} mol cm^{-3}), and v is the scan rate (mV s^{-1}).

Figure 8 represents the CVs of the modified electrode, GC/Pd-SB, in a solution of (50 μM of paracetamol + 0.1 M PBS (pH = 7.4)) at a wide range of scan rates (5–150 mV s^{-1}). The inset figure showed the linear relation between the oxidation peak current vs. the scan rate's square root. The diffusion coefficients for paracetamol were estimated as 1.18×10^{-6} cm^2 s^{-1}.

Table 3 The electrochemical equivalent circuit parameters of GC/Pd-SB electrodes in a solution of 0.1 M PBS in the presence and absence of 50 μM of paracetamol

Electrode	Element	R_s	R_1	C_1	R_2	C_2	W	
	Unit	Ohm.cm^2	Ohm.cm^2	μF.cm^2	Ohm.cm^2	μF.cm^2	mMho s$^{1/2}$	χ^2
Absence of paracetamol		3.840	3032.040	0.9499	6506.874	6.838	0.605×10^{-4}	0.0246
Presence of paracetamol		1.1806	526.835	2.1917	653.692	26.884	1.390×10^{-4}	0.0595

Fig. 7 a CVs of GC/Pd-SB in different concentrations of paracetamol solution and 0.1 M PBS (pH = 7.4) at scan rate 20 mV.s^{-1}. **b** Linear relation between anodic peak current versus the paracetamol concentration
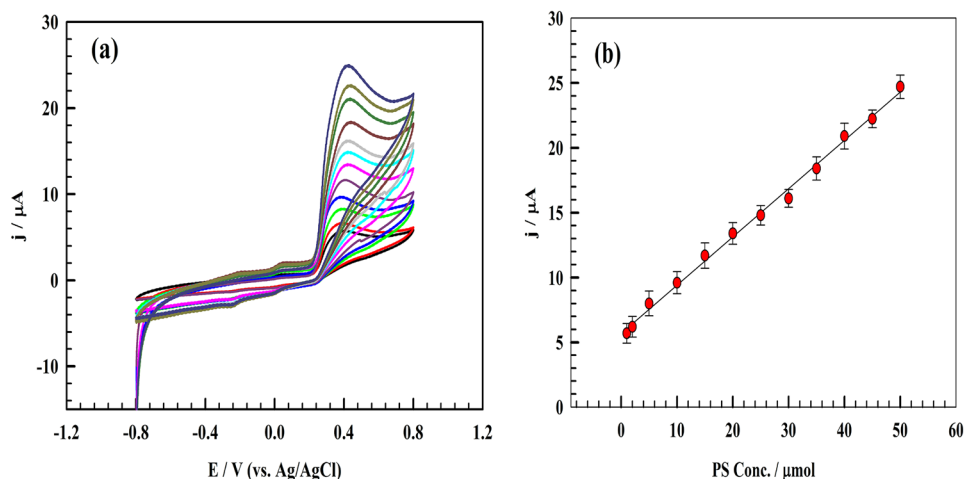

Table 4 Comparison between different electrodes for detection of paracetamol

Electrocatalyst	Linearity range (μM)	Limit of detection (μM)	Measurement technique	Ref
γ-Fe$_2$O$_3$/CNTs	2.5 – 385	0.046	Differential pulse voltammetry	[71]
Pd nanorods@C-S-doped	0.033 –120	0.011	Differential pulse voltammetry	[72]
3D graphene-carbon nanotubes− AuPd nanoparticles	0.10 to 10	0.050	Differential pulse voltammetry	[73]
Pt/CeO2@Cu2O-CPE	0.4–32	0.05	Cyclic voltammetry	[74]
ZnO/FMWCNT/CPE	0.5–13	0.23	Cyclic voltammetry	[75]
Au-rGO@poly (L-cysteine)	1–200	0.5	Cyclic voltammetry	[76]
Pd-SB	1–50	0.067	Cyclic voltammetry	This work
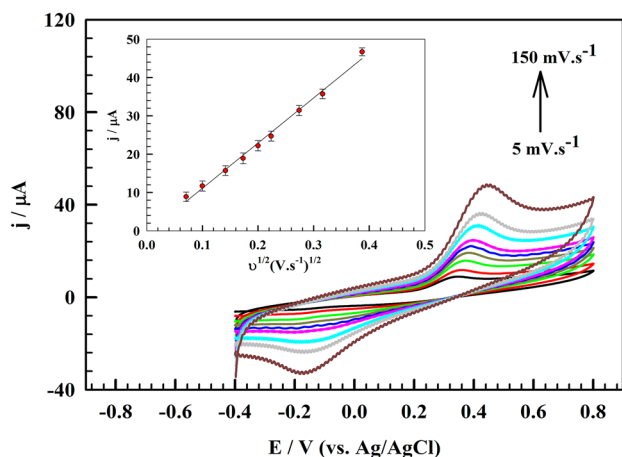
Fig. 8 CVs of 50 μM paracetamol/0.1 M PBS/pH 7.0 recorded at different scan rate values from 5 to 150 mV. s^{-1}. Inset: plot of the anodic peak current of paracetamol as a function of the square root of scan rate

Durability of Electrodes

The high density of ionic charges in the self-assembly leads to enhancing the stability and strength of the materials. One of the significant disadvantages of the self-assembly molecule is that the strong ionic interactions also decrease the opportunities for relaxation and rearrangements [77].

The modified electrode's stability toward the oxidation was utilized using 20 repeated CVs in a solution of 0.1 M phosphate buffer and 50 μM paracetamol at a scan rate of 20 mV s^{-1}. As displayed in Fig. 9a, a slight significant decrease in peak current was observed, indicating the electrode's high durability toward continuous oxidation. The chronoamperometry technique was carried out at the oxidation peak potential for each compound to measure its stability as a function of constant potential oxidation, and the chronoamperograms were represented in Fig. 9b, where the current decreased by 6% after 10 min of continuous oxidation.
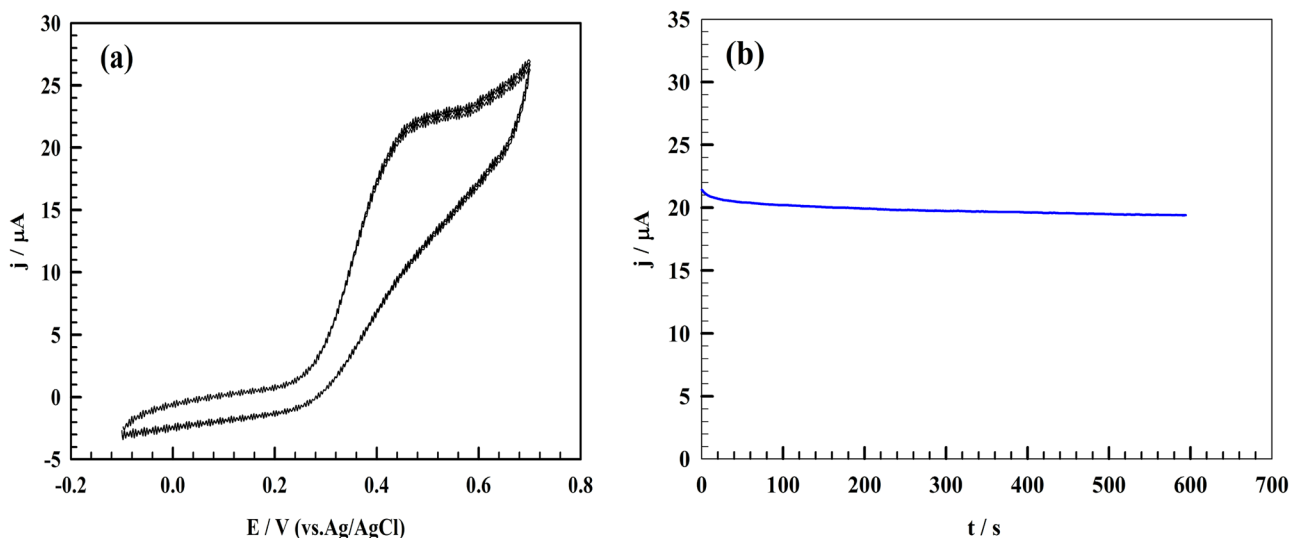
Fig. 9 **a** Repeated 20 CVs of GC/Pd-SB in solution of 50 μM of paracetamol and 0.1 M PBS (pH= 7.4) at scan rate of 20 mV.s-1, **b** Chronoamperometery at constant oxidation potential 500 mV (vs.Ag/AgCl)

The electrode's operative durability was utilized by continually testing the same electrode in the buffer solution containing 50 μm of paracetamol ten times. Thus, the electrode exhibits nearly the same response (RSD=0.418%, SD=0.8433, $n=10$), which reflects the excellent reproducibility of the modified electrode.

Effect of pH

The effect of pH was performed to find out the best measurement environment for electrochemical determination where the average pH value of blood is ca. 7.4 and urine ca. 4.5–8 [78, 79]. Figure 10 shows the linear sweep voltammetry for modified GC/Pd-SB for different pH values ranging 4 up to 9 at a scan rate of 20 mV s^{-1} in a solution of 50 μM of paracetamol and 0.1 M PBS. The oxidation peak current was found to be changed as the pH of the solution changed. The best oxidation peak current was achieved at pH 7.

In contrast, the current in the acidic medium is likely to be higher than that in the basic medium due to the stability of the Pd complex being more in the acidic medium, as given in Fig. 11a.

A direct relationship was found between the oxidation peak potential and the solution's pH. The anodic peak potential, E_p, was found to be shifted more negatively with increasing pH value as shown in Fig. 11b according to the following equation:

$$E_p = 0.95 - 0.064 \, pH_{Paracetamol}, \ R^2 = 0.993$$

where the value of the linear relation is approached to the Nernstian slope value.

The pKa value of paracetamol is 9.4 [78]. The relation between pH and oxidation peak current was investigated and indicated the effect of medium pH on the activity of the electrochemical process for the GC/Pd-SB sensor.

Interference Study

The electrode's selectivity toward paracetamol was investigated against another interfering molecule in biological fluids like dopamine, uric acid, and glucose using chronoamperometry at the paracetamol oxidation potential of 0.5 V (vs. Ag/AgCl). As represented in
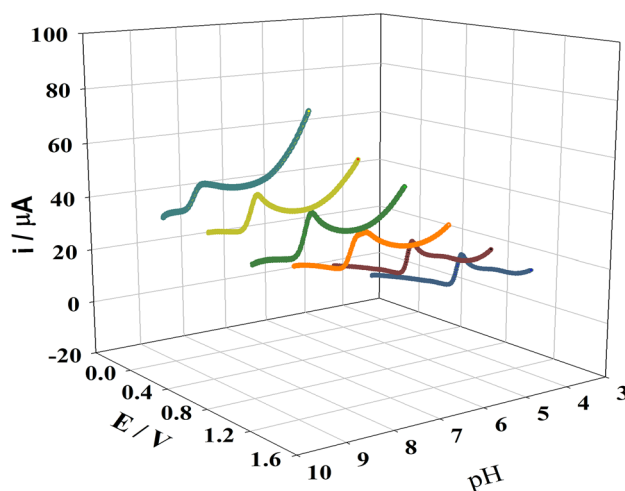

Fig. 10 LSV of modified Pd-Schiff base electrode at the solution of 50 μM paracetamol in 0.1 M phosphate buffer at different pH values
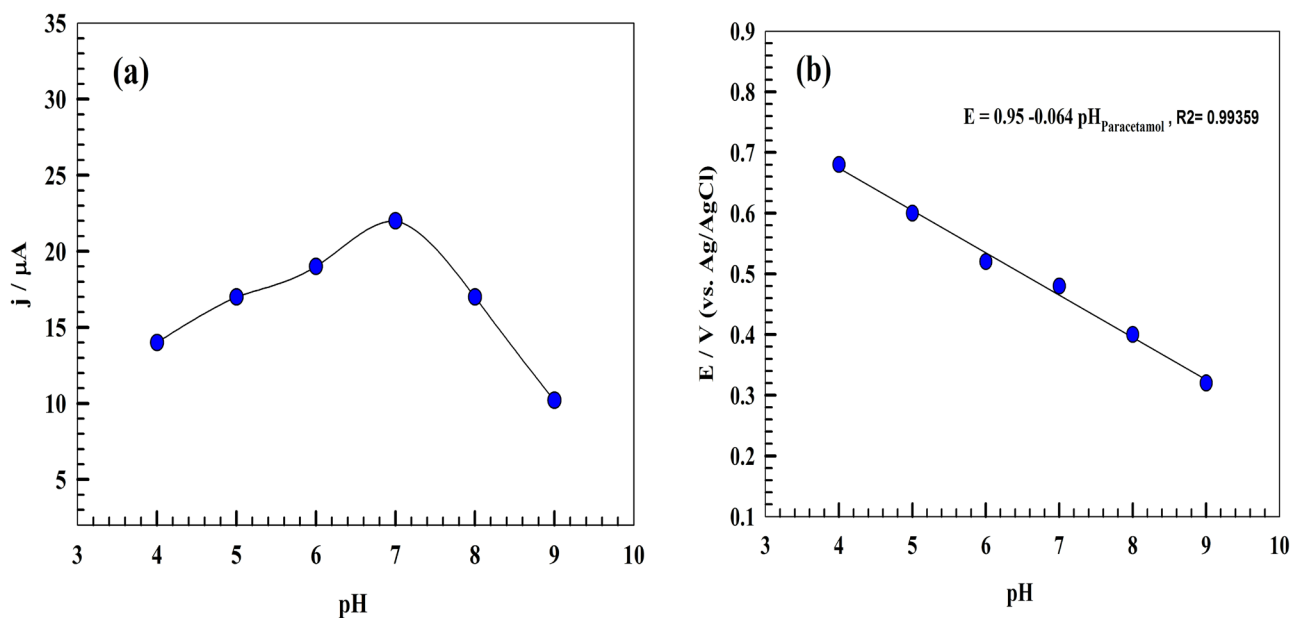
Fig. 11 **a** The relation between pH and oxidation peak current. **b** Relation between the pH of solution and oxidation peak potential

Fig. 12a, the electrode exhibits significant activity by sequential addition of 10 µM of paracetamol and interfering compounds with concentrations equaled 50 µM. Thus, the electrode showed high anti-interference ability for paracetamol detection in the presence of other interference species like KCl, ascorbic acid (AA), uric acid (UA), dopamine (DP), and glucose (Glu). The normalized current is illustrated in Fig. 12b. Thus, the addition of KCl increased the current by ~ 1.3% because of the enhancement of solution conductivity by the effect of strong electrolytes. The increase in current by ascorbic acid and uric acid is due to the correlation between the oxidation potential of species and paracetamol.
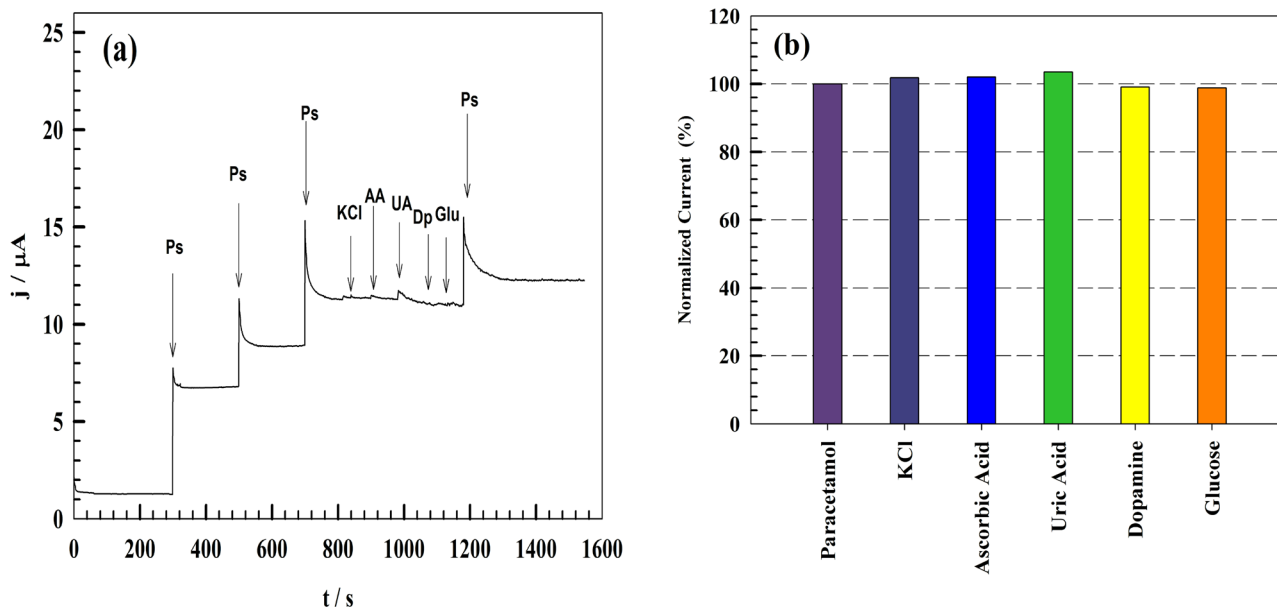

Fig. 12 **a** Interference study by chronoamperometry at constant potential +500 mV (vs. Ag/AgCl) for different interfering materials in biological fluids like KCl, ascorbic acid (AA), uric acid (UA), dopa- mine (DP), and glucose(Glu). **b** Normalized current in the presence of paracetamol and other interfering species

Table 5 Real sample electrochemical detection of paracetamol

Studied compound	Concentration of added (μmol L^{-1})	Concentration of found (μmol L^{-1})	Recovery (%)	RSD (%)
Paracetamol	45	45.5	101.1	0.325
	65	64.6	99.3	0.347
	110	112	101.8	0.805
	120	119.3	99.4	0.422

On the other hand, the adsorption of dopamine and glucose on the electrode surface blocks the electrode's activity toward paracetamol oxidation. Consequently, the dopamine and glucose presence reduces the electrode current by ~ 1.2%. According to the previous result, the activity corresponding to the modified palladium electrode has high non-interfering properties.

Real Sample Determination

The sample of paracetamol was spiked to a human serum collected freshly. The serum specimens were centrifuged, filtrated, and diluted via PBS pH = 7.4 and spiked by different paracetamol concentrations [80] and were measured using a modified GC/Pd-Schiff base electrode. Originally, drugs containing paracetamol (Panadol tablet 500 mg/tablet) were purchased from the market and used to prepare stock solutions. Different paracetamol concentrations were prepared in a 0.1 M PBS of pH 7.4. The anodic peak current was measured using LSV and compared using the calibration curve, and the recovery results are shown in Table 5.

Conclusion

A simple electrochemical sensor based on a Pd-Schiff base was investigated for paracetamol detection. Self-assembly Pd complex showed a unique electrocatalytic activity toward paracetamol detection in phosphate buffer solution owing to the high electronic and magnetic properties.

In the modified glassy carbon, GC/Pd-SB, the electrode was found to have excellent activity toward determining paracetamol in PBS with a detection limit of 0.067 μM and linear detection limit in the range of 1–50 μM. Otherwise, the anti-interference ability of the electrode was proved in the presence of dopamine, uric acid, and glucose. The recovery of the modified electrode using a commercial paracetamol tablet was acceptable. Finally, the Pd-Schiff base complex is a promising sensor for detecting paracetamol with a small detection limit and acceptable with a range of pH values because of the high structural stability of the self-assembly metal complex. The paracetamol adsorption upon palladium

centers studied as a function of adsorption energy with a high negative value reflects the preference of the paracetamol to be adsorbed onto the Pd centers.

Declarations

References

1. T. Teker, M. Aslanoglu, Microchem. J. **158**, 105234 (2020)
2. B. Avinash, C.R. Ravikumar, M.R.A. Kumar, H.P. Nagaswarupa, M.S. Santosh, A.S. Bhatt, D. Kuznetsov, J. Phys. Chem. Solids **134**, 193 (2019)
3. K. Chetankumar, B.E.K. Swamy, S.C. Sharma, Microchem. J. **160**, 105729 (2021)
4. T.S.S.K. Naik, B.E.K. Swamy, P.C. Ramamurthy, K. Chetankumar, Mater. Sci. Energy Technol. **3**, 626 (2020)
5. S. Bhattacharyya, K. Yan, L. Pence, P.M. Simpson, P. Gill, L.G. Letzig, R.D. Beger, J.E. Sullivan, G.L. Kearns, M.D. Reed, Biomark. Med. **8**, 147 (2014)
6. I. Dalmázio, T. Alves, R. Augusti, J. Braz. Chem. Soc. **19**, 81 (2008)
7. W. Lohmann, U. Karst, Anal. Bioanal. Chem. **386**, 1701 (2006)
8. S. Emdadi, M.H. Sorouraddin, L. Denanny, Analyst **146**, 1326 (2021)
9. M. Iranifam, S. Khodaei, M. Saadati, Microchem. J. **146**, 850 (2019)
10. G.G. Oliveira, B.C. Janegitz, M.B. Batistão, F.H. Salami, O. Fatibello-Filho, O.D. Leite, Quim. Nova **32**, 1755 (2009)
11. T. Borahan, T. Unutkan, A. Şahin, S. Bakırdere, J. Sep. Sci. **42**, 678 (2019)

12. P. Chandra, A.S. Rathore, S. Lohidasan, K.R. Mahadik, Sci. Pharm. **80**, 337 (2012)
13. A.K. Hewavitharana, S. Lee, P.A. Dawson, D. Markovich, P.N. Shaw, Anal. Biochem. **374**, 106 (2008)
14. J. Meyer, U. Karst, Chromatographia **54**, 163 (2001)
15. M. de los A Oliva, R.A. Olsina, A.N. Masi, Talanta **66**, 229 (2005)
16. J.A. Arancibia, A.J. Nepote, G.M. Escandar, A.C. Olivieri, Anal. Chim. Acta **419**, 159 (2000)
17. M.H. Hasan, M.E. El-sadek, S.M. El-Adl, Anal. Chem. Lett. **11**, 427 (2021)
18. R.M.S. Hameed, S.S. Medany, Microchem. J. **145**, 354 (2019)
19. N.A. El-Nabarawy, K.M. Zohdy, S.S. Medany, S.A. Fadlallah, Microchem. J. **153**, 104398 (2020)
20. R.M.A. Hameed, S.S. Medany, Synth. Met. **247**, 67 (2019)
21. R.M.A. Hameed, S.S. Medany, Appl. Surf. Sci. **458**, 252 (2018)
22. S.A. Wring, J.P. Hart, Analyst **117**, 1215 (1992)
23. J.-M. Zen, A. Senthil Kumar, D.-M. Tsai, Electroanalysis **15**, 1073 (2003)
24. V.F. Lotfy, S.S. Hassan, P.A. Khalf-Alla, A.H. Basta, Int. J. Polym. Mater. Polym. Biomater. **69**, 21 (2020)
25. S.S. Hassan, S.M. Gomha, Chem. Pap. **73**, 331 (2019)
26. S.N. Shukla, P. Gaur, M.L. Raidas, B. Chaurasia, J. Mol. Struct. **1202**, 127362 (2020)
27. N. Shahabadi, S. Kashanian, F. Darabi, Eur. J. Med. Chem. **45**, 4239 (2010)
28. S. Alexander, V. Udayakumar, V. Gayathri, J. Mol. Catal. A Chem. **314**, 21 (2009)
29. M.M. El-Hendawy, A.E.-M.M. Ramadan, M.M. Ibrahim, Int. J. Hydrogen Energy **46**, 39786 (2021)
30. M. Arshadi, M. Ghiaci, A. Gil, Ind. Eng. Chem. Res. **50**, 13628 (2011)
31. S. Moradinasab, M. Behzad, Desalin. Water Treat. **57**, 4028 (2016)
32. H.-T. Feng, Y.-S. Zheng, Chem. – A Eur. J. **20**, 195 (2014)
33. N. Lemberger, J. Almog, J. Forensic Sci. **52**, 1107 (2007)
34. R. Rozin, J. Almog, Forensic Sci. Int. **208**, 25 (2011)
35. L.S. De Oliveira, A.P. dos Santos Poles, M.A. Balbino, M.M. Teles de Menezes, J.F. De Andrade, E.R. Dockal, H.M. Tristão, M.F. De Oliveira, Sensors **13**, 7668 (2013)
36. M.F. Muzetti Ribeiro, J.W. de Cruz Júnior, E.R. Dockal, B.R. McCord, M.F. de Oliveira, Electroanalysis **28**, 320 (2016)
37. L.S. de Oliveira, M.A. Balbino, M.M.T. de Menezes, E.R. Dockal, M.F. de Oliveira, Microchem. J. **110**, 374 (2013)
38. Y. Teng, R. Liu, C. Li, H. Zhang, J. Hazard. Mater. **192**, 1766 (2011)
39. I. Oh, R.I. Masel, Electrochem. Solid-State Lett. **10**, J19 (2007)
40. X. Wang, B. He, J. Nie, W. Yin, H. Fa, C. Chen, Res. Chem. Intermed. **44**, 6689 (2018)
41. A. John, L. Benny, A.R. Cherian, S.Y. Narahari, A. Varghese, G. Hegde, J. Nanostructure Chem. **11**, 1 (2021)
42. S. Dutta, C. Ray, S. Mallick, S. Sarkar, A. Roy, T. Pal, RSC Adv. **5**, 51690 (2015)
43. T.Y. Tekbaşoğlu, T. Soganci, M. Ak, A. Koca, M.K. Şener, Biosens. Bioelectron. **87**, 81 (2017)
44. L. Lamiri, O. Belgherbi, C. Dehchar, S. Laidoudi, A. Tounsi, B. Nessark, F. Habelhames, A. Hamam, B. Gourari, Synth. Met. **266**, 116437 (2020)
45. P. Kumar, V. Kumar, R. Gupta, Dalt. Trans. **46**, 10205 (2017)
46. S.S. Hassan, P.A. Khalf-Alla, Appl. Organomet. Chem. **34**, e5432 (2020)
47. M.J. Frisch, http://www.Gaussian.com/ (2009)
48. B. Hammer, L.B. Hansen, J.K. Nørskov, Phys. Rev. B **59**, 7413 (1999)
49. S.J. Clark, M.D. Segall, C.J. Pickard, P.J. Hasnip, M.I.J. Probert, K. Refson, M.C. Payne, Zeitschrift Für Krist. Mater. **220**, 567 (2005)
50. H.J. Monkhorst, J.D. Pack, Phys. Rev. B **13**, 5188 (1976)
51. S. Menati, H. Amiri Rudbari, B. Askari, M. Riahi Farsani, F. Jalilian, G. Dini, Comptes Rendus Chim. **19**, 347 (2016)
52. H. Wang, X. Nie, X. Guo, C. Song, J. CO2 Util. **15**, 107 (2016)
53. Y. Ren, M.-Y. Li, Y.-X. Song, M.-Y. Sui, G.-Y. Sun, X.-C. Qu, P. Xie, J.-L. Lu, J. Photochem. Photobiol. A Chem. **407**, 113087 (2021)
54. A.S. Rad, M. Ardjmand, M.R. Esfahani, B. Khodashenas, Spectrochim. Acta Part A Mol. Biomol. Spectrosc. **247**, 119082 (2021)
55. M. Sankarganesh, R. Vijay Solomon, J. Dhaveethu Raja, J. Biomol. Struct. Dyn. **39**, 1055 (2021)
56. A. Aykan, O. Karaman, C. Karaman, A. Necip, M.L. YOLA, Surf. Interfaces **25**, 101293 (2021)
57. C.C. Boungou, G.B. Bouka-Pivoteau, B.R. Malonda-Boungou, M. N'dollo, P.S. Moussounda, A.T. Raji, E. Kanga, Comput. Condens. Matter **28**, e00582 (2021)
58. X. Cui, J. Liu, X. Yan, Y. Yang, B. Xiong, Appl. Surf. Sci. **570**, 151234 (2021)
59. J.W. McBain, D.G. Hopkins, J. Phys. Chem. **29**, 188 (2002)
60. S.S. Voyutskii, J. Adhes. **3**, 69 (1971)
61. B.V. Derjaguin, V.P. Smilga, J. Appl. Phys. **38**, 4609 (1967)
62. T. Semoto, Y. Tsuji, K. Yoshizawa, J. Phys. Chem. C **115**, 11701 (2011)
63. A. Dąbrowski, Adv. Colloid Interface Sci. **93**, 135 (2001)
64. K. Duanmu, D.G. Truhlar, J. Phys. Chem. C **118**, 28069 (2014)
65. P.-H. Liu, F.-T. Tsai, B.-H. Chen, I.-J. Hsu, H.-H. Hsieh, W.-F. Liaw, Dalt. Trans. **48**, 6040 (2019)
66. W.-K. Chen, S.-H. Liu, M.-J. Cao, Q.-G. Yan, C.-H. Lu, J. Mol. Struct. THEOCHEM **770**, 87 (2006)
67. X. Kang, J. Wang, H. Wu, J. Liu, I.A. Aksay, Y. Lin, Talanta **81**, 754 (2010)
68. F. Shihana, D. Dissanayake, P. Dargan, A. Dawson, Clin. Toxicol. **48**, 42 (2010)
69. B. Saad, M.F. Bari, M.I. Saleh, K. Ahmad, M.K.M. Talib, J. Chromatogr. A **1073**, 393 (2005)
70. C. Gardana, M. Scaglianti, P. Pietta, P. Simonetti, J. Pharm. Biomed. Anal. **45**, 390 (2007)
71. X.-Q. Cai, K. Zhu, B.-T. Liu, Q.-Y. Zhang, Y.-H. Luo, D.-E. Zhang, J. Electrochem. Soc. **168**, 57511 (2021)
72. L. Wang, Y. Yang, H. Liang, N. Wu, X. Peng, L. Wang, Y. Song, J. Hazard. Mater. **409**, 124528 (2021)
73. L. Yang, B. Zhang, B. Xu, F. Zhao, B. Zeng, Talanta **224**, 121845 (2021)
74. A.R. Rajamani, S.C. Peter, A.C.S. Appl, Nano Mater. **1**, 5148 (2018)
75. M. Kumar, B.E.K. Swamy, S. Reddy, W. Zhao, S. Chetana, V.G. Kumar, J. Electroanal. Chem. **835**, 96 (2019)
76. L. Zhang, X. Si, X. Yan, H. He, D. Deng, L. Luo, Curr. Anal. Chem. **16**, 1063 (2020)
77. S. Datta, M.L. Saha, P.J. Stang, Acc. Chem. Res. **51**, 2047 (2018)
78. V. Bernal, A. Erto, L. Giraldo, J.C. Moreno-Piraján, Molecules **22**, 1032 (2017)
79. R.K. Packer, W.A. Dunson, J. Exp. Zool. **174**, 65 (1970)
80. T. Iranmanesh, M.M. Foroughi, S. Jahani, M.S. Zandi, H.H. Nadiki, Talanta **207**, 120318 (2020)